

SetONet: A Deep Set-based Operator Network for Solving PDEs with permutation invariant variable input sampling

Stepan Tretiakov^{a,*}, Xingjian Li^b, Krishna Kumar^{a,b}

^aMaseeh Department of Civil, Architectural and Environmental Engineering, University of Texas at Austin, Austin, 78712, TX, USA

^bOden Institute for Computational Engineering and Sciences, University of Texas at Austin, Austin, 78712, TX, USA

Abstract

Neural operators, particularly the Deep Operator Network (DeepONet), have shown promise in learning mappings between function spaces for solving differential equations. However, standard DeepONet requires input functions to be sampled at a fixed set of locations, limiting its applicability in scenarios with variable sensor configurations, missing data, or irregular grids. To address this limitation, we introduce the Set Operator Network (SetONet), a novel architecture that integrates Deep Sets principles into the DeepONet framework. The core innovation lies in the SetONet branch network, which processes the input function as an unordered *set* of location-value pairs $\{(\mathbf{x}_i, g(\mathbf{x}_i))\}_{i=1}^M$. This design ensures permutation invariance with respect to the input points, making SetONet inherently robust to variations in the number (M) and locations (\mathbf{x}_i) of sensors. By explicitly processing both spatial coordinates and function values, SetONet learns richer, spatially-aware input representations. We demonstrate SetONet's effectiveness on several benchmark problems, including derivative/anti-derivative operators, 1D Darcy flow, and 2D elasticity. Results show that SetONet successfully learns operators under variable input sampling conditions where standard DeepONet fails. Furthermore, SetONet is architecturally robust to sensor drop-off; unlike standard DeepONet, which requires methods like interpolation to function with missing data. Notably, SetONet can also achieve comparable or improved accuracy over DeepONet on fixed grids, particularly for nonlinear problems, likely due to its enhanced input representation. SetONet provides a flexible and robust extension to the neural operator toolkit, significantly broadening the applicability of operator learning to problems with variable or incomplete input data.

Keywords: Operator Learning, Neural Operators, Deep Sets, DeepONet, PDE Modeling

1. Introduction

Neural operators train deep neural networks to learn mappings between infinite-dimensional function spaces to approximate the solution operators of differential equations [1]. They take input functions—such as coefficients, boundary conditions, or forcing terms—and output the corresponding solution functions. Several distinct architectural approaches exist. Meta-architectures, such as the Deep Operator Network (DeepONet) [2], employ separate networks for processing input functions and query locations, inspired by operator approximation theorems [3]. Integral transform-based operators often parameterize integral kernels in transformed domains; examples include the Fourier Neural Operator (FNO) [4], Wavelet Neural Operator (WNO) [5], Graph Kernel Network (GKN) [6], and Laplace Neural Operator (LNO) [7]. More recently, transformer-based operators like the Operator Transformer (OFormer) [8] and the General Neural Operator Transformer (GNOT) [9] utilize attention mechanisms adapted from sequence modeling.

The objective in operator learning is typically to learn a single mapping that generalizes across a range of scenarios, such as different domain geometries, input parameters, or initial and boundary conditions associated with the underlying ordinary differential equation or partial differential equation (ODE/PDE) system. However, achieving this

*Corresponding author.

Email addresses: stepan@utexas.edu (Stepan Tretiakov), xingjian.li@austin.utexas.edu (Xingjian Li), krishnak@utexas.edu (Krishna Kumar)

goal faces challenges with certain architectures. A significant limitation, particularly for standard DeepONet [10, 2], is the reliance on a fixed input structure. Specifically, the branch network, responsible for encoding the input function, typically requires function evaluations at a predetermined and consistent set of sensor locations across all samples [11, 12].

This fixed-input requirement hinders applications where input data originates from variable sensor configurations. Such scenarios arise naturally when sensor placements differ between experiments, sensor counts fluctuate due to failures or design choices, or data is inherently defined on irregular grids [11]. Standard DeepONet cannot directly process these variable-length or variably located input sets.

To address this limitation, we introduce the Set Operator Network (SetONet). SetONet modifies the DeepONet framework to explicitly handle variable input sampling by incorporating principles from Deep Sets [13]. The core innovation lies in the SetONet branch network, which processes the input function as an unordered set of location-value pairs $\{(\mathbf{x}_i, g(\mathbf{x}_i))\}_{i=1}^M$. The size M of this set can vary.

By employing Deep Sets methodology, the SetONet branch achieves permutation invariance. This means its output encoding of the input function g is independent of the order of the location-value pairs and robust to variations in the number of points M . Furthermore, SetONet explicitly uses both location \mathbf{x}_i and value $g(\mathbf{x}_i)$ information within its branch network. This allows it to learn spatially-aware input representations, potentially improving accuracy even when input locations are fixed, particularly for problems with complex spatial dependencies.

This paper introduces the Set Operator Network (SetONet) architecture, designed to learn operators effectively from variable input discretizations. We demonstrate its capabilities and robustness compared to standard DeepONet, particularly in scenarios involving varying sensor locations and sensor drop-off. To achieve this, we first review related approaches for handling variable inputs in section 2. We then detail the proposed SetONet architecture and its components in section 3.4. Subsequently, section 4 presents comparative experimental results on several benchmark PDE problems, evaluating performance under different input sampling conditions. Finally, section 5 summarizes our findings and discusses potential directions for future research.

The code developed for this study will be made available on GitHub upon publication.

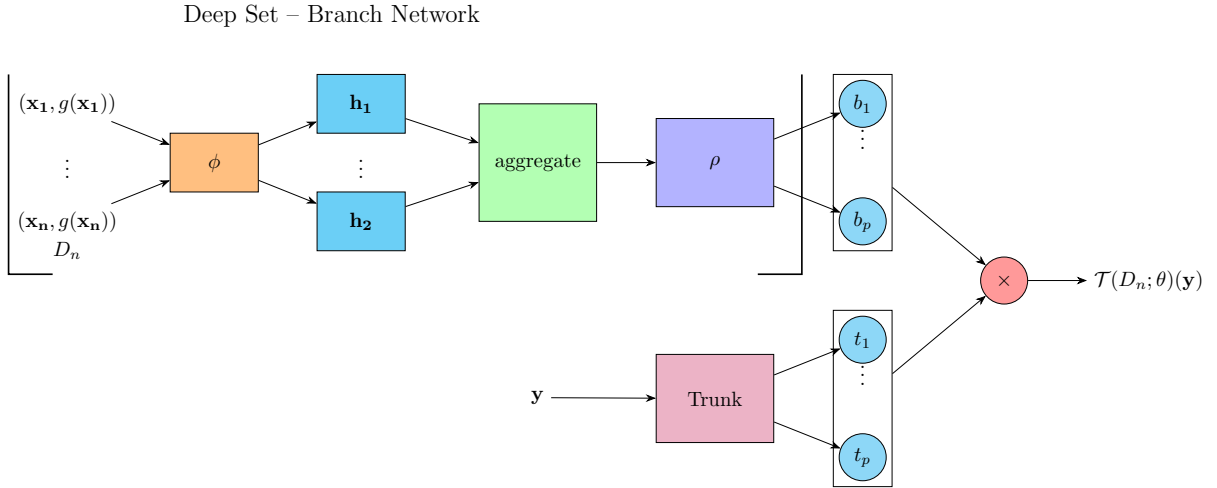


Figure 1: Schematic of the proposed Set Operator Network (SetONet) architecture for solving PDEs with variable input sampling. The branch network (top) leverages Deep Sets principles [13] to process the input function represented as an unordered *set* of M location-value pairs $\{(\mathbf{x}_i, g(\mathbf{x}_i))\}_{i=1}^M$. This involves an element-wise transformation ϕ applied to each pair (potentially after positional encoding, see Sec. 3.5), a permutation-invariant aggregation step (e.g., mean or attention pooling), and a final set-level transformation ρ to produce latent branch coefficients $\mathbf{b} = [\mathbf{b}_1, \dots, \mathbf{b}_p]$. Concurrently, the trunk network (bottom) maps the query location \mathbf{y} to corresponding basis vectors $\mathbf{t}(\mathbf{y}) = [\mathbf{t}_1(\mathbf{y}), \dots, \mathbf{t}_p(\mathbf{y})]$. The final operator approximation $\hat{\mathcal{T}}(g)(\mathbf{y})$ is computed by combining \mathbf{b} and $\mathbf{t}(\mathbf{y})$ as detailed in Eq. (6).

2. Related Work

The standard Deep Operator Network (DeepONet) architecture [10, 2], while powerful for learning operators between function spaces, typically requires input functions to be sampled at a fixed and consistent set of locations for its branch network [11, 12]. This limitation hinders its direct application in scenarios where sensor placements vary across experiments, sensor numbers change, or data is inherently irregular [11]. Consequently, several research efforts have focused on extending DeepONet or developing related neural operator architectures to handle variable input sampling.

A direct approach involves designing architectures specifically for variable inputs. The Variable-Input Deep Operator Network (VIDON) [11] explicitly addresses this challenge. VIDON processes sets of input coordinate-value pairs $\{(\mathbf{x}_j, g(\mathbf{x}_j))\}_{j=1}^m$, where the number of points m can vary. It employs separate MLPs to encode coordinates and values, combines them, and then uses a multi-head attention-like mechanism inspired by Transformers to produce a fixed-size representation of the input function, irrespective of m . Crucially, VIDON is permutation invariant with respect to the input points and has been proven to be a universal approximator for continuous operators even with variable inputs. Empirical results show its robustness across various irregular sampling scenarios, including missing data and random sensor placements.

Another significant line of research leverages attention mechanisms, known for their ability to handle variable-length sequences and focus on relevant input parts. Integrating attention into the DeepONet branch network allows the model to dynamically weight input sensor readings based on their importance or location [14]. This dynamic weighting can adapt to varying numbers and positions of sensors. Specific implementations include using attention layers within the BranchNet for tasks like nonlinear fiber transmission simulation [14]. Furthermore, concepts like orthogonal attention have been proposed to build neural operators robust to irregular geometries [15]. Architectures like the Latent Neural Operator (LNO) utilize a Physics-Cross-Attention module, enabling operation in a latent space and prediction at arbitrary locations, implicitly handling variable inputs [16]. Other attention-based operators like ONO [15], PIANO [17], CoDA-NO [18], and Kernel-Coupled Attention [19] further underscore the utility of attention for flexible input handling in operator learning.

In a more recent work, the Resolution Independent Neural Operator (RINO) [20] proposes an alternative approach that also handles input functions sampled at different coordinates. Instead of directly using function values, a set of neural network-parameterized basis functions is learned to approximate the input function space. The DeepONet architecture then takes the corresponding projection coefficients, obtained via implicit neural representations as input, enabling it to process functions with varying resolutions. Similar ideas are also explored in [12] with bigger deviation from the standard DeepONet framework.

Graph Neural Networks (GNNs) offer a natural framework for processing data defined on irregular domains or point clouds, making them suitable for variable input sampling [21]. Input samples can be represented as nodes in a graph, with features corresponding to function values and edges representing spatial relationships (e.g., proximity). GNNs integrated into the DeepONet branch network can learn features by aggregating information from neighboring sample points via message passing, inherently handling variations in the number and arrangement of points. Hybrid models combining GNNs and DeepONet have demonstrated success. For example, GraphDeepONet uses a GNN for temporal evolution on irregular grids while DeepONet captures spatial characteristics [21, 22]. MeshGraphNet has shown promise for flow fields on irregular grids [23], and Point-DeepONet integrates PointNet (a GNN for point clouds) to process 3D geometries directly [22]. These works establish GNNs as a viable method for equipping DeepONet with variable and irregular input capabilities.

Finally, alternative architectural modifications have been explored. Fusion DeepONet [23] employs neural field concepts and modifies the branch-trunk interaction to improve generalization on irregular grids, outperforming standard DeepONet in such settings. Its ability to handle arbitrary grids suggests flexibility towards variable input locations. As mentioned earlier, Latent Neural Operators (LNOs) [16] operate in a learned latent space, decoupling the operator learning from the physical input grid and allowing decoding at arbitrary points, which inherently supports variable input structures. These examples show that fundamental changes to the DeepONet structure or operating paradigm can also yield architectures capable of handling non-standard input sampling.

Collectively, these approaches demonstrate significant progress in overcoming the original DeepONet’s fixed input sampling limitation, utilizing dedicated designs, attention mechanisms, graph neural networks, and other architectural innovations.

3. SetONet for PDE Modeling

Having established the motivation and reviewed related work, this section details the proposed Set Operator Network (SetONet) methodology. We begin by outlining the necessary preliminaries, including the standard DeepONet framework that SetONet extends. We then introduce the core concepts of Deep Sets, which enable permutation-invariant processing. Finally, we present the complete SetONet architecture, detailing its branch and trunk network components and how they operate on set-structured inputs.

3.1. Preliminaries

Before introducing the SetONet architecture, we first establish the mathematical context for operator learning and briefly review the standard Deep Operator Network (DeepONet) framework upon which our method builds. This includes defining the objective of learning mappings between function spaces and outlining the typical structure and input requirements of DeepONet’s branch and trunk networks.

3.2. Deep operator network (DeepONet)

We adopt the Deep Operator Network (DeepONet) framework to approximate the solution operator \mathcal{T} of the governing PDE, which maps the input function space \mathcal{G} to the output function space \mathcal{H} . Let $\Omega \subset \mathbb{R}^D$ be a bounded open set in the physical space, and let $\mathcal{G} = \mathcal{G}(\Omega_x; \mathbb{R}^{d_x})$ and $\mathcal{H} = \mathcal{H}(\Omega_y; \mathbb{R}^{d_y})$ be two separable functional spaces for which the mapping is to be learned. Furthermore, let $\mathcal{T} : \mathcal{G} \rightarrow \mathcal{H}$ denote the linear or nonlinear mapping arising from the solution of an unknown static or time-dependent PDE. The objective of an operator learning task is to approximate the target operator via the following parametric mapping

$$\mathcal{T} : \mathcal{G} \times \Theta \rightarrow \mathcal{H} \quad \text{or more commonly,} \quad \mathcal{T}_\theta : \mathcal{G} \rightarrow \mathcal{H}, \quad \theta \in \Theta, \quad (1)$$

where Θ is a finite-dimensional parameter space and θ represents the set of trainable parameters. The optimal parameters θ^* are learned by training a neural operator with backpropagation based on a labeled dataset obtained through simulation or experiment.

The standard DeepONet architecture comprises two parallel deep neural networks—a *branch network* and a *trunk network* working together to construct the target operator. The branch network processes the input function $g \in \mathcal{G}$ sampled at m fixed sensor locations $\{\mathbf{x}_i\}_{i=1}^m$, yielding a feature vector $\mathbf{b}(g)$. Simultaneously, the trunk network takes as input the spatial and temporal coordinates $(\mathbf{x}, t) \in \Omega_y$, producing a coordinate feature vector $\mathbf{t}(\mathbf{x}, t)$. The DeepONet approximation of the solution operator \mathcal{T} for a given input g_1 is then constructed via the inner product of these features:

$$\mathcal{T}_\theta(g_1)(\mathbf{x}_j, t_j) = \sum_{i=1}^p b_i(g_1) \cdot t_i(\mathbf{x}_j, t_j), \quad (2)$$

where $\mathbf{b} = [b_1, b_2, \dots, b_p]^T$ is the output vector of the branch net, and $\mathbf{t} = [t_1, t_2, \dots, t_p]^T$ is the output vector of the trunk net and p denotes a hyperparameter that controls the size of the output layer of both the branch and trunk networks. The trainable parameters of the DeepONet, represented by θ in eq. (2), which parameterize both the branch network and the trunk network, are obtained by minimizing a data-driven loss function, which is expressed as:

$$\mathcal{L}(\theta) = \min_{\theta} \|\mathcal{T}_\theta(g)(\mathbf{x}, t) - \mathcal{T}(g)(\mathbf{x}, t)\|_2^2, \quad (3)$$

where $\mathcal{T}_\theta(g)(\mathbf{x}, t)$ is the prediction of the DeepONet and $\mathcal{T}(g)(\mathbf{x}, t)$ is the ground truth of the solution obtained from either experimental measures or by using a standard numerical solver. In practice, the branch and trunk networks can be modeled with any DNN architecture. Here, we primarily consider a fully connected feed-forward neural network, also referred to as a multi-layer perceptron (MLP), for both networks (branch and trunk).

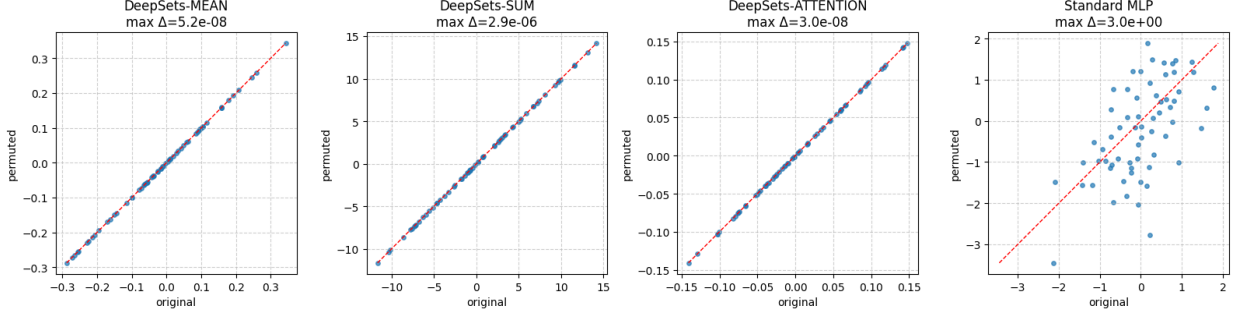


Figure 2: Permutation-invariance test for Deep Sets with three aggregation functions (MEAN, SUM, ATTENTION, left to right) and a standard MLP branch network (far right). Each panel plots the model’s output on a randomly permuted input set (vertical axis) against its output on the original ordering (horizontal axis); the red dashed line indicates perfect invariance.

3.3. Deep Sets

We briefly describe the deep sets method proposed in [13]. Deep Sets is a neural network framework designed to operate on set-valued inputs, ensuring that the learned function is *permutation invariant*, that is, the output of the model remains unchanged under any permutation of input elements (Fig. 2). Formally, for any set $X = \{\mathbf{x}_1, \mathbf{x}_2, \dots, \mathbf{x}_M\} \subset \mathbb{R}^d$ and any permutation π of indices $\{1, \dots, M\}$, a function $f : 2^{\mathbb{R}^d} \rightarrow \mathbb{R}$ is permutation invariant if:

$$f(\{\mathbf{x}_1, \mathbf{x}_2, \dots, \mathbf{x}_M\}) = f(\{\mathbf{x}_{\pi(1)}, \mathbf{x}_{\pi(2)}, \dots, \mathbf{x}_{\pi(M)}\}). \quad (4)$$

Deep Sets models any such function f using the following structure:

$$f(X) = \rho \left(\sum_{\mathbf{x} \in X} \phi(\mathbf{x}) \right), \quad (5)$$

where the function can be broken into three key components:

- **Element-wise transformation** $\phi : \mathbb{R}^d \rightarrow \mathbb{R}^k$: maps each element of the input set to a latent representation. This captures instance-level features in a shared, permutation-independent manner.
- **Aggregation** $\sum_{\mathbf{x} \in X} \phi(\mathbf{x})$: combines the element-wise representations into a single global feature vector. The summation operator also ensures permutation invariance. Alternative aggregations (e.g., mean or attention (discussed in Section 3.5.1)) can be used depending on the task.
- **Set-level transformation** $\rho : \mathbb{R}^k \rightarrow \mathbb{R}$: processes the aggregated representation to produce the final output.

Here we note that $\phi : \mathbb{R}^d \rightarrow \mathbb{R}^k$ and $\rho : \mathbb{R}^k \rightarrow \mathbb{R}$ are typically implemented as neural networks and optimized in training. notably the original deep sets also provided an alternative architecture for permutation equivariance functions (i.e., the output reorders according to the input permutation), however, we will omit this here as it is beyond the scope of this work.

3.4. The SetONet Framework

While the DeepONet architecture presented in Section 3.1 provides a powerful and general framework for learning operators, its standard implementation often relies on evaluating the input function $g \in \mathcal{G}$ over a predetermined, fixed set of sensor locations $\{\mathbf{x}_i\}_{i=1}^m$. This requirement for fixed sensor points can be restrictive in various practical settings where sensor positions may vary or data might be incomplete. Furthermore, the branch network in conventional DeepONets typically processes only the vector of sensor values $[g(\mathbf{x}_1), \dots, g(\mathbf{x}_m)]$, implicitly relying on the fixed input structure to associate values with locations, which can limit its ability to capture complex spatial dependencies within the input function.

To overcome these limitations, we introduce the Set Operator Network (SetONet), an architecture that synergistically combines the operator learning capabilities of DeepONet with the permutation-invariant processing power of

Deep Sets [13] (discussed in Section 3.1). A key conceptual shift in SetONet is the reformulation of the branch network to operate on the input function data represented as an unordered set of location-value pairs $\{(\mathbf{x}_i, g(\mathbf{x}_i))\}_{i=1}^M$, where M represents the potentially variable number of sensor readings.

Notably, unlike standard DeepONet branches, the SetONet branch explicitly processes both the spatial coordinates \mathbf{x}_i and the corresponding function values $g(\mathbf{x}_i)$ jointly within its initial feature extraction layers (detailed in Section 3.5). This explicit incorporation of spatial information alongside functional values allows the branch network to learn a significantly richer and more spatially-aware representation of the input function g . By directly processing the geometric information, the branch can more effectively model local variations, correlations, and the overall structure of the input function, leading to a more informative latent encoding.

Building upon this enhanced input representation, the SetONet branch leverages the Deep Sets methodology to ensure permutation invariance with respect to the input set $\{(\mathbf{x}_i, g(\mathbf{x}_i))\}_{i=1}^M$. This property guarantees that the learned function encoding is independent of the sensor ordering and makes the architecture naturally robust to variations in the number (M) and locations (\mathbf{x}_i) of sensors. This combination of explicit spatial feature extraction and permutation invariance primarily offers enhanced flexibility for handling variable input discretizations. Moreover, the improved representational capacity can contribute to superior performance in certain contexts; for instance, as observed in our results (Section 4), this allows SetONet to outperform standard DeepONet on problems characterized by significant nonlinearity or complex spatial structure, such as the 1D Darcy flow benchmark, even when evaluated using fixed sensor locations.

SetONet maintains the fundamental two-component structure of DeepONet. The permutation-invariant, spatially-aware branch network produces a latent representation encoding the input function g , while a separate trunk network processes the query locations $\mathbf{y} \in \Omega_y$ where the output $\mathcal{T}(g)(\mathbf{y})$ is desired. The outputs of these two networks are then combined, usually via a dot product analogous to Equation (2), to yield the final operator approximation. The subsequent section provides a detailed description of the specific architectural components and mechanisms employed within the SetONet framework, highlighting its effective integration of these principles.

3.5. SetONet Architecture

The SetONet architecture adheres to the two-component structure of DeepONet, consisting of a branch network and a trunk network, whose outputs are combined to approximate the target operator \mathcal{T} . The branch network, however, is specifically designed using Deep Sets principles to process input function data as a set of location-value pairs. We show the diagram for the proposed method in fig. 1. Let the input function $g \in \mathcal{G}$ be represented by M sensor readings $\{(\mathbf{x}_i, \mathbf{u}_i)\}_{i=1}^M$, where $\mathbf{x}_i \in \mathbb{R}^{d_x}$ are the sensor locations with dimensionality d_x , and $\mathbf{u}_i = g(\mathbf{x}_i) \in \mathbb{R}^{d_u}$ are the corresponding sensor values with dimensionality d_u . The output $\mathcal{T}(g)(\mathbf{y})$ is queried at locations $\mathbf{y} \in \mathbb{R}^{d_y}$, where d_y is the dimensionality of the query coordinates. The final output has dimensionality d_{out} .

3.5.1. Branch Network

The branch network transforms the input set $\{(\mathbf{x}_i, \mathbf{u}_i)\}_{i=1}^M$ into a fixed-size latent representation \mathbf{b} that encodes the input function g . This process involves four stages: input processing with optional positional encoding, an element-wise transformation network (ϕ), an aggregation layer, and a final transformation network (ρ).

Input Processing and Positional Encoding (PE):. To leverage the spatial information \mathbf{x}_i , SetONet can incorporate positional encoding before the ϕ network. The location \mathbf{x}_i is transformed into a positional feature vector \mathbf{e}_i , which is then concatenated with the sensor value \mathbf{u}_i . Based on the experiments conducted, two options are relevant:

- **No Positional Encoding:** The raw location vector is used directly, $\mathbf{e}_i = \mathbf{x}_i$. The input to the ϕ network for sensor i is the concatenation $[\mathbf{x}_i; \mathbf{u}_i] \in \mathbb{R}^{d_x+d_u}$.
- **Sinusoidal Positional Encoding:** This technique embeds the coordinates $\mathbf{x}_i \in \mathbb{R}^{d_x}$ into a higher-dimensional space $\mathbb{R}^{d_{pe}}$ using a deterministic function based on sine and cosine waves of multiple frequencies [24]. The purpose is to generate a fixed representation of position that allows the model to easily reason about relative spatial arrangements. The embedding dimension d_{pe} must be an even integer divisible by d_x . Let $d'_{pe} = d_{pe}/d_x$ denote the number of dimensions allocated to represent each single coordinate component. A set of frequencies $\{\omega_l\}_{l=0}^{(d'_{pe}/2)-1}$ is defined using a geometric progression: $\omega_l = f_{base}^{2l/d'_{pe}}$, where f_{base} is a chosen base frequency (e.g.,

$1/10000$ or related to a maximum positional scale hyperparameter f_{max}). For each component $x_{i,j}$ ($j = 1, \dots, d_x$) of the input coordinate vector \mathbf{x}_i , a sub-vector is computed by applying sine and cosine functions with these frequencies:

$$\mathbf{e}_{i,j} = [\sin(\omega_0 x_{i,j}), \cos(\omega_0 x_{i,j}), \dots, \sin(\omega_{(d'_{pe}/2)-1} x_{i,j}), \cos(\omega_{(d'_{pe}/2)-1} x_{i,j})] \in \mathbb{R}^{d'_{pe}}$$

The complete positional embedding $\mathbf{e}_i \in \mathbb{R}^{d_{pe}}$ is formed by concatenating these sub-vectors for all input dimensions: $\mathbf{e}_i = [\mathbf{e}_{i,1}; \mathbf{e}_{i,2}; \dots; \mathbf{e}_{i,d_x}]$. This multi-frequency representation captures positional information across different scales. Crucially, for any fixed offset k , the encoding $\text{PE}(x+k)$ can be represented as a linear transformation of $\text{PE}(x)$, making it straightforward for attention mechanisms or MLPs to learn relative positioning [24]. The resulting embedding \mathbf{e}_i is concatenated with the sensor value \mathbf{u}_i , forming the input vector $[\mathbf{e}_i; \mathbf{u}_i] \in \mathbb{R}^{d_{pe}+d_u}$ for the ϕ network.

This explicit handling of spatial coordinates via PE allows the network to be sensitive to the locations of the sensor readings.

Element-wise Transformation (ϕ): Each concatenated input vector (incorporating location/PE and value) is processed independently by a shared Multi-Layer Perceptron (MLP), denoted as the ϕ network. This network maps each input vector to an intermediate latent representation $\mathbf{h}_i \in \mathbb{R}^{d_\phi}$, where d_ϕ is the latent dimension of the ϕ network's output. The ϕ network is implemented as an MLP consisting of several hidden layers with a chosen nonlinear activation function (e.g., ReLU).

Aggregation: To obtain a single, fixed-size representation for the entire input set while ensuring permutation invariance, the individual latent representations $\{\mathbf{h}_i \in \mathbb{R}^{d_\phi}\}_{i=1}^M$ generated by the ϕ network are aggregated into a vector \mathbf{h}_{agg} . This crucial step pools information across all sensor readings, summarizing the state represented by the set of sensors. The two aggregation methods employed in our study are:

- **Mean Aggregation:** This is the simplest strategy, where all sensor representations are treated with equal importance. The representations are averaged element-wise:

$$\mathbf{h}_{agg} = \frac{1}{M} \sum_{i=1}^M \mathbf{h}_i$$

The resulting aggregated vector \mathbf{h}_{agg} resides in \mathbb{R}^{d_ϕ} , maintaining the same dimensionality d_ϕ as the individual representations \mathbf{h}_i . While straightforward, this method cannot adaptively focus on potentially more informative sensor readings within the set.

- **Attention Pooling:** To enable a more adaptive aggregation strategy, we employ an attention mechanism based on the Pooling by Multihead Attention (PMA) concept from the Set Transformer [25], configured with a single pooling token ($k = 1$). This approach introduces a single learnable query parameter vector $\mathbf{q} \in \mathbb{R}^{d_\phi}$. Unlike the sensor representations \mathbf{h}_i , which depend on the current input data, \mathbf{q} is an intrinsic parameter of the pooling module, optimized globally during model training.

To understand its function intuitively, consider the set $\{\mathbf{h}_i\}$ as a collection of informative documents specific to the current input function g . The learnable vector \mathbf{q} acts as a refined 'research query' that the model learns, through training, is most effective for probing this collection to extract task-relevant information. The attention mechanism then functions like a targeted retrieval system:

- i) The learned \mathbf{q} serves as the Query.
- ii) Representations derived from $\{\mathbf{h}_i\}$ serve as the Keys, against which the Query is compared to determine relevance.
- iii) Other representations derived from $\{\mathbf{h}_i\}$ serve as the Values, which contain the information to be aggregated.

The mechanism calculates attention weights α_i based on the similarity between the Query \mathbf{q} and the Keys derived from each \mathbf{h}_i . These weights quantify the relevance of each document \mathbf{h}_i to the learned research query \mathbf{q} . The final aggregated vector \mathbf{h}_{agg} is computed as a weighted average of the Value vectors \mathbf{v}_i (derived from $\{\mathbf{h}_i\}$), using these attention weights: $\mathbf{h}_{agg} = \sum_{i=1}^M \alpha_i \mathbf{v}_i$.

Thus, $\mathbf{h}_{agg} \in \mathbb{R}^{d_\phi}$ represents a synthesized summary of the input set, specifically tailored by the interaction between the learned query \mathbf{q} and the current sensor representations $\{\mathbf{h}_i\}$. This allows the model to dynamically assign importance to different sensor readings based on the learned query, offering greater flexibility than uniform averaging, while producing a final summary vector of the same dimension d_ϕ .

Set-level Transformation (ρ): Finally, the aggregated representation \mathbf{h}_{agg} is processed by another MLP, the ρ network. This network maps the fixed-size aggregated vector to the final raw branch output $\mathbf{b}_{raw} \in \mathbb{R}^{p \times d_{out}}$, where p is the latent dimension shared with the trunk network, and d_{out} is the final output dimensionality. The ρ network is implemented as an MLP comprising hidden layers with nonlinear activations. This raw output is then reshaped into the branch coefficients \mathbf{b} (shape (p, d_{out}) for a single sample).

3.5.2. Trunk Network

Complementary to the branch network, the trunk network processes the coordinates \mathbf{y} at which we want to evaluate the output of the learned operator $\mathcal{T}(g)(\mathbf{y})$. The input \mathbf{y} represents a location in the output domain (with dimensionality d_y). The trunk network is implemented as a standard Multi-Layer Perceptron (MLP) with several hidden layers and nonlinear activation functions. Its primary role is to generate a set of p basis functions, denoted collectively as $\mathbf{t}(\mathbf{y})$, whose values depend on the specific query location \mathbf{y} . For each query point \mathbf{y} , the trunk network computes p corresponding basis vectors, each having the same dimensionality d_{out} as the final output $\mathcal{T}(g)(\mathbf{y})$. The number of layers, the size of the hidden layers, and the specific activation function are hyperparameters of the model.

3.5.3. Output Computation

The final prediction $\hat{\mathcal{T}}(g)(\mathbf{y}) \in \mathbb{R}^{d_{out}}$ is constructed by combining the information encoded in the branch network's output coefficients \mathbf{b} (which capture the nature of the input function g) and the trunk network's basis functions $\mathbf{t}(\mathbf{y})$ (which depend on the query location \mathbf{y}).

Recall that the branch network produces p coefficient vectors (collectively \mathbf{b}), each of dimension d_{out} , and for a given query point \mathbf{y} , the trunk network produces p corresponding basis vectors (collectively $\mathbf{t}(\mathbf{y})$), also each of dimension d_{out} . The core computation involves pairing the k -th coefficient vector from the branch with the k -th basis vector from the trunk (for k from 1 to p).

Specifically, the output $\mathcal{T}(g)(\mathbf{y})$ (before adding the optional bias) is calculated as the sum of element-wise products between corresponding branch and trunk vectors over the latent dimension p :

$$\mathcal{T}(g)(\mathbf{y}) = \sum_{k=1}^p \mathbf{b}_k \odot \mathbf{t}_k(\mathbf{y}) \quad (6)$$

where $\mathbf{b}_k \in \mathbb{R}^{d_{out}}$ is the k -th coefficient vector from the branch, $\mathbf{t}_k(\mathbf{y}) \in \mathbb{R}^{d_{out}}$ is the k -th basis vector from the trunk evaluated at \mathbf{y} , and \odot denotes element-wise multiplication. This sum essentially reconstructs the output function at \mathbf{y} using the p basis functions generated by the trunk, weighted by the coefficients determined by the branch from the input function g .

This architecture enables SetONet to learn operator mappings effectively, accommodating set-structured inputs with potentially variable sensor configurations and explicitly leveraging spatial information through positional encoding.

4. Results and Discussion

In this section, we evaluate the performance of the proposed SetONet architecture against the standard DeepONet baseline on a series of benchmark problems. We aim to demonstrate SetONet's ability to handle variable input sampling and its robustness compared to DeepONet. The experiments cover fundamental calculus operators (derivative

and anti-derivative), a nonlinear 1D Darcy flow problem, and a 2D elasticity problem. For each benchmark, we compare the architectures under different input conditions, including training with fixed versus variable sensor locations and evaluating robustness to sensor drop-off at test time.

4.1. Derivative and Anti-Derivative Operators

We first evaluate the performance of SetONet and DeepONet on two related benchmark tasks based on fundamental calculus operators: differentiation and integration. These operators, while relatively simple, serve as valuable initial benchmarks in one dimension. Their well-defined mathematical properties allow for a clear and controlled assessment of the core operator learning capabilities of the architectures, particularly in evaluating their robustness and performance under different input sampling conditions, such as fixed versus variable sensor locations and scenarios with sensor drop-off.

First, we consider learning the derivative operator. For this task, the input function space consists of cubic polynomials, $p_3(x)$, and the output function space comprises the corresponding quadratic polynomials, $p_2(x)$, obtained by differentiation. The goal is to learn the operator $\mathcal{T}_{\text{deriv}} : p_3(x) \mapsto p_2(x)$ where $p_2(x) = \frac{dp_3(x)}{dx}$ for each function in the input space.

Second, we address the inverse task: learning the anti-derivative (integral) operator. Here, the input function space consists of quadratic polynomials, $p_2(x)$, and the output function space contains the corresponding cubic polynomials, $p_3(x)$, such that $p_2(x)$ is the derivative of $p_3(x)$. Specifically, we aim to learn the operator $\mathcal{T}_{\text{int}} : p_2(x) \mapsto p_3(x)$ where $\frac{dp_3(x)}{dx} = p_2(x)$ and we assume the constant of integration is zero (i.e., $p_3(0) = 0$).

We now proceed to discuss the results for both operator learning tasks under these various experimental conditions.

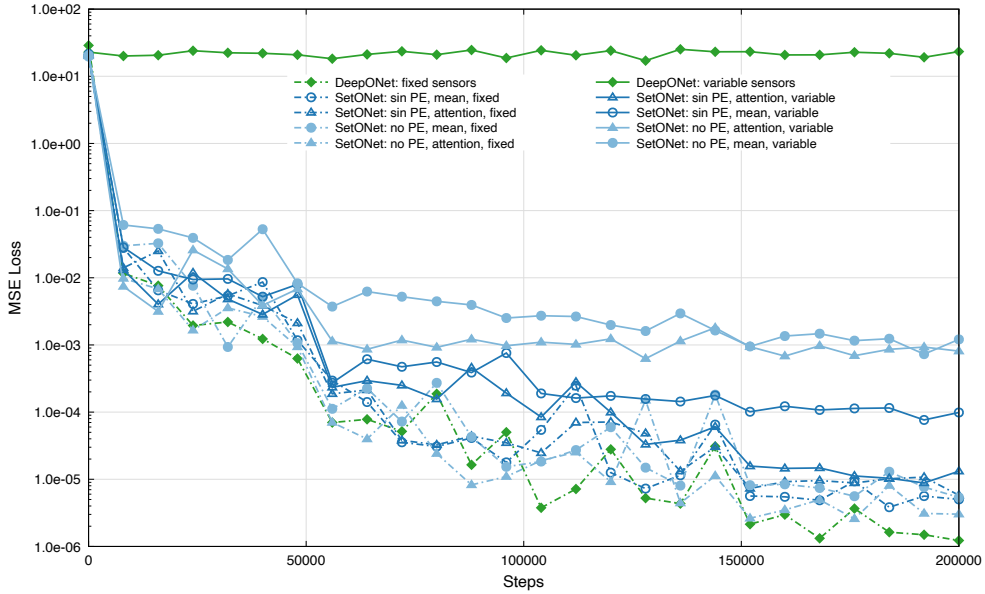


Figure 3: Test performance (Mean Squared Error Loss vs. Steps) for DeepONet and SetONet architectures on the Derivative approximation benchmark. Results are shown for models trained under two sensor sampling conditions: fixed locations per batch (dashed lines, "fixed") and randomly resampled locations per batch (solid lines, "variable"). Within each condition, the performance of DeepONet can be compared to SetONet variants incorporating different positional encoding (sinusoidal/none) and aggregation (attention/mean) methods.

Derivative Operator Results

We begin by evaluating the models on the task of learning the derivative operator mapping cubic polynomials to their quadratic derivatives. The quantitative performance is summarized in Table 1 (Relative L_2 error), with convergence behavior shown in the loss curves (Figs. 3, 5) and qualitative predictions illustrated (Figs. 4 and 7)

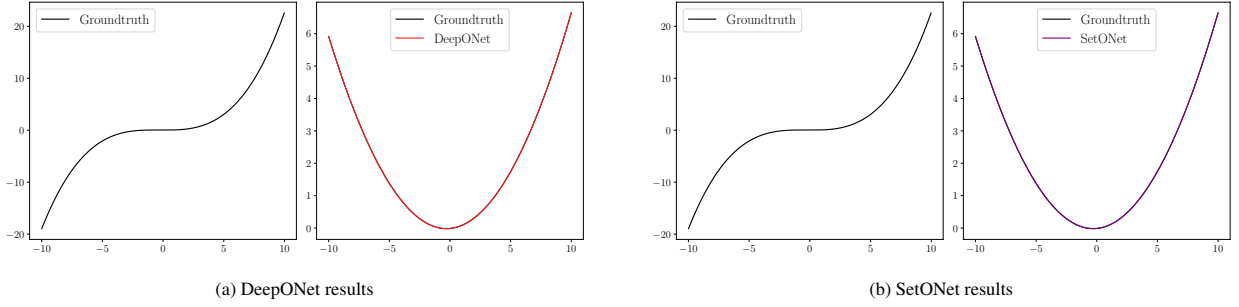


Figure 4: Comparison of DeepONet and SetONet results on the Derivative approximation benchmark. Left: Approximation results for DeepONet. Right: Approximation results for SetONet. In each subfigure we show both the source function as well as the predicted output function.

Table 1: Comparison of Relative L_2 Error for DeepONet and SetONet variants on the Derivative approximation benchmark. Models were trained with either variable (randomly resampled per batch) or fixed sensor locations. The final column shows performance under test-time sensor drop-off (20%) for models originally trained with fixed sensors.

Model	Variable Sensors	Fixed Sensors	Fixed w/ 20% Drop-off
DeepONet	-	6.48×10^{-4}	3.04×10^{-2}
SetONet (PE: Sin, Agg: Att)	1.70×10^{-3}	9.89×10^{-4}	5.90×10^{-2}
SetONet (PE: Sin, Agg: Mean)	4.28×10^{-3}	9.37×10^{-4}	1.01×10^{-1}
SetONet (PE: None, Agg: Att)	6.80×10^{-3}	8.47×10^{-4}	1.57×10^{-2}
SetONet (PE: None, Agg: Mean)	1.07×10^{-2}	1.29×10^{-3}	7.44×10^{-2}

Performance with Fixed Sensor Locations. We first evaluate performance under the "fixed" condition. In this setup, a single specific set of sensor locations was initially sampled randomly (resulting in a non-uniform spatial distribution), and importantly, this same fixed set of locations was used consistently for evaluating every function sample during both training and testing (dashed lines, Fig. 3; Table 1, Col. 2). Under these conditions where the sampling locations are consistent across inputs, both the standard DeepONet and all tested SetONet configurations demonstrate high accuracy. The Relative L_2 errors for all models are consistently low, on the order of 10^{-3} or 10^{-4} . DeepONet achieves a relative L_2 error of 6.48×10^{-4} , serving as a strong baseline. Among the SetONet variants, the configuration using no positional encoding and attention aggregation (PE: None, Agg: Att) achieves the lowest relative L_2 error at 8.47×10^{-4} , performing essentially on par with the standard DeepONet. Other SetONet configurations yield slightly higher but still comparable relative L_2 errors (up to 1.29×10^{-3}). Qualitative examples (Fig. 4) visually confirm the high fidelity of the predictions for both architectures in this setting. This baseline case demonstrates that both architectures achieve high accuracy when the input function sampling is consistent across examples, even if the fixed locations themselves are randomly distributed, with the best SetONet configuration performing comparably to DeepONet.

Table 2: Comparison of Relative L_2 Error for DeepONet and SetONet variants on the Integral approximation benchmark. Models were trained with either variable (randomly resampled per batch) or fixed sensor locations. The final column shows performance under test-time sensor drop-off (20%) for models originally trained with fixed sensors.

Model	Variable Sensors	Fixed Sensors	Fixed w/ 20% Drop-off
DeepONet	-	7.61×10^{-4}	3.87×10^{-2}
SetONet (PE: Sin, Agg: Att)	9.84×10^{-3}	1.65×10^{-3}	5.05×10^{-2}
SetONet (PE: Sin, Agg: Mean)	1.09×10^{-2}	2.63×10^{-3}	2.00×10^{-1}
SetONet (PE: None, Agg: Att)	3.56×10^{-3}	1.05×10^{-3}	3.57×10^{-2}
SetONet (PE: None, Agg: Mean)	1.11×10^{-2}	2.57×10^{-3}	2.21×10^{-1}

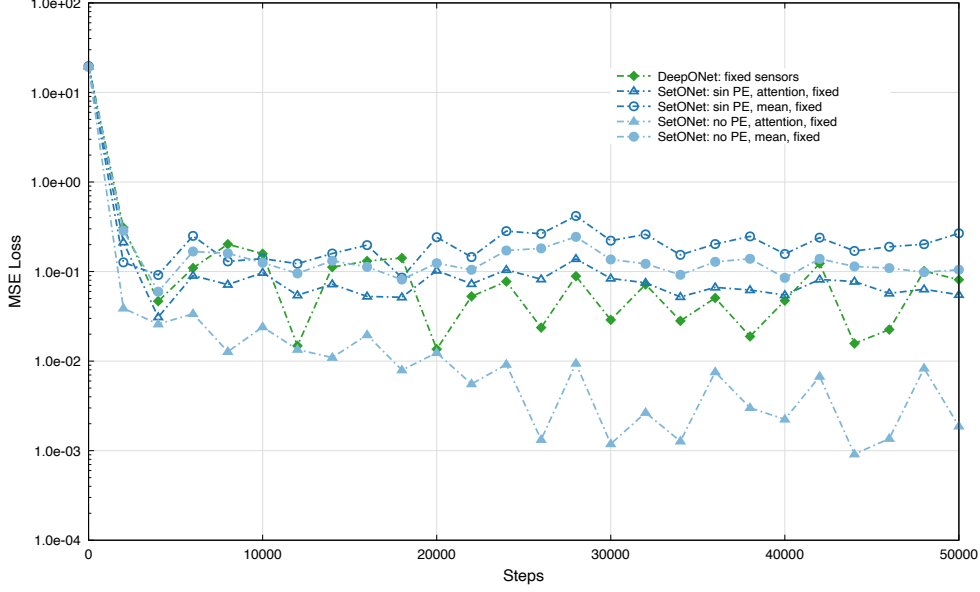


Figure 5: Test performance (Mean Squared Error Loss vs. Steps) for DeepONet and SetONet architectures on the Derivative approximation benchmark, evaluated on a test set where 20% of sensors were randomly dropped out at test time only. All models were trained using fixed sensor locations per batch (dashed lines, "fixed"). The plot allows a comparison of DeepONet against SetONet variants (incorporating different positional encoding (sinusoidal/none) and aggregation (attention/mean) methods) under this specific test condition with sensor dropout.

Performance with Variable Sensor Locations. The necessity for architectures capable of handling flexible inputs becomes evident when training with variable sensor locations, where sensor positions are randomly resampled for each training batch ("variable" condition; solid lines, Fig. 3; Table 1, Col. 1). Standard DeepONet, constrained by its fixed input structure, fails to learn the operator, indicated by the lack of a converged relative L_2 error metric (Table 1, Col. 1). In contrast, all SetONet variants successfully learn the operator, achieving low relative L_2 errors. This highlights the effectiveness of SetONet's permutation-invariant branch design for handling input sets with varying discretizations encountered across different batches. Among the SetONet configurations, those employing sinusoidal positional encoding (PE: Sin) yield the lowest relative L_2 errors (1.70×10^{-3} for Att, 4.28×10^{-3} for Mean), substantially outperforming variants without PE (6.80×10^{-3} and 1.07×10^{-2}). This finding underscores the importance of explicitly encoding spatial information when sensor locations vary dynamically during training. Furthermore, attention aggregation demonstrates a slight advantage over mean aggregation when combined with sinusoidal PE in this scenario. The qualitative result in Fig. 4 (b) illustrates SetONet's accurate prediction capability even when trained under this variable per-batch sensor sampling strategy.

Robustness to Sensor Drop-off. To assess robustness to incomplete data at inference time, models trained with fixed sensors were evaluated on test sets where 20% of the randomly distributed fixed sensors were randomly removed (Fig. 5; Table 1, Col. 3). Standard DeepONet, by design, requires a complete input vector corresponding to the fixed sensor locations and cannot inherently process incomplete sets. Therefore, for this test, missing sensor values for DeepONet were estimated using linear interpolation based on the known sensor positions before being input to the network. While performance degrades for all models compared to the baseline fixed-sensor case, the impact is more pronounced for DeepONet (relative L_2 error increases from 6.48×10^{-4} to 3.04×10^{-2}), suggesting that linear interpolation on this non-uniform sensor distribution may not fully recover the necessary information for accurate prediction. SetONet, conversely, processes the reduced sensor set directly without interpolation, leveraging its inherent permutation-invariant architecture designed to handle variable inputs. Although SetONet errors also increase, the variant using no PE and attention aggregation (PE: None, Agg: Att) demonstrates the best robustness, achieving a relative L_2 error (1.57×10^{-2}) significantly lower than the interpolated DeepONet result. This highlights SetONet's architectural advantage in directly handling missing data, outperforming DeepONet even when the latter uses imputation,

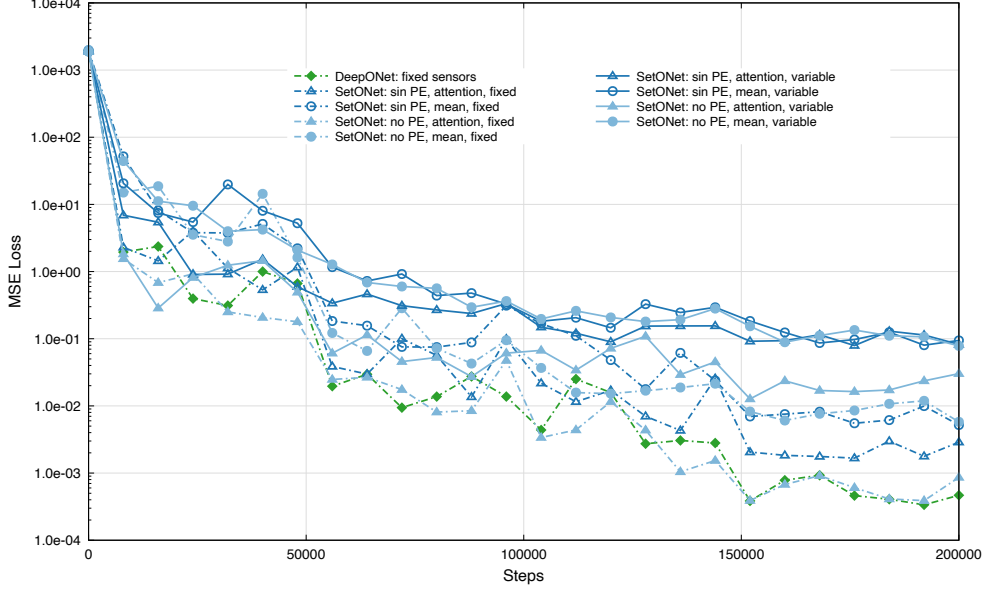


Figure 6: Test performance (Mean Squared Error Loss vs. Steps) for DeepONet and SetONet architectures on the Integral approximation benchmark. Results are shown for models trained under two sensor sampling conditions: fixed locations per batch (dashed lines, "fixed") and randomly resampled locations per batch (solid lines, "variable"). Within each condition, the performance of DeepONet can be compared to SetONet variants incorporating different positional encoding (sinusoidal/none) and aggregation (attention/mean) methods.

particularly when interpolation is challenged by non-uniform sensor distributions.

Anti-Derivative (Integral) Operator Results

Next, we evaluate the task of learning the anti-derivative operator, mapping quadratic polynomials ($p_2(x)$) to their corresponding cubic integrals ($p_3(x)$) such that $dp_3/dx = p_2(x)$. The results are presented in Table 2 and Figures 6, 7, 8.

Performance with Fixed Sensor Locations. In the "fixed" condition, where sensor locations were fixed at the same set of randomly sampled, non-uniformly distributed points for all inputs (dashed lines, Fig. 6; Table 2, Col. 2), standard DeepONet performs well, achieving a relative L_2 error of 7.61×10^{-4} . For this integral operator task under fixed sampling, DeepONet achieves a slightly lower error compared to the tested SetONet variants, whose relative L_2 errors range from 1.05×10^{-3} to 2.63×10^{-3} . The SetONet configuration without positional encoding and using attention aggregation (PE: None, Agg: Att) is the most competitive among the SetONet options, with a relative L_2 error of 1.05×10^{-3} , which is comparable to the DeepONet baseline. Qualitative results (Fig. 7) illustrate good predictive accuracy for both architectures under these ideal fixed sampling conditions. This result confirms that the standard DeepONet architecture remains a highly effective baseline when input sampling is consistent.

Performance with Variable Sensor Locations. Consistent with the derivative task, standard DeepONet fails entirely when trained with variable sensor locations resampled per batch ("variable" condition; solid lines, Fig. 6; Table 2, Col. 1), indicated by the lack of a converged relative L_2 error metric (Table 2, Col. 1). Conversely, all SetONet variants demonstrate their ability to handle this variable sampling, successfully learning the operator with relative L_2 errors ranging from 3.56×10^{-3} to 1.11×10^{-2} . This again highlights the advantage of SetONet's permutation-invariant architecture. Notably, the best performing SetONet variant for this task under variable sampling utilizes no positional encoding and attention aggregation (PE: None, Agg: Att), achieving the lowest relative L_2 error of 3.56×10^{-3} . Unlike the derivative case, sinusoidal positional encoding did not provide a clear benefit for learning the integral operator under variable sampling in these experiments.

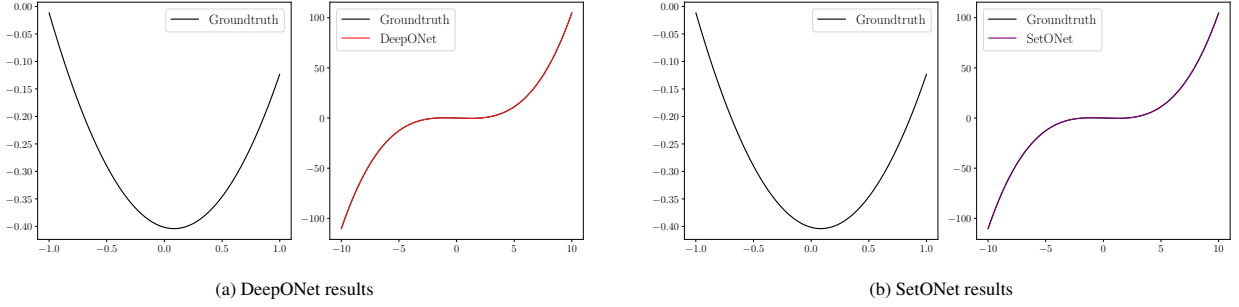


Figure 7: Comparison of example predictions for the Integral approximation benchmark. Left (a): DeepONet prediction (red) vs. ground truth (black). Right (b): SetONet prediction (purple) vs. ground truth (black). Both models demonstrate high accuracy on this task when trained with fixed sensors. The input quadratic function and the target cubic function are shown in the left panel of each subfigure’s included graphic.

Robustness to Sensor Drop-off. Evaluating models trained on fixed sensors against test data with 20% sensor drop-off (Fig. 8; Table 2, Col. 3), we again assess robustness to inference-time data loss. As standard DeepONet requires a complete input vector by design, missing values were estimated using linear interpolation based on the known, non-uniform sensor locations. DeepONet’s relative L_2 error increases substantially (from 7.61×10^{-4} to 3.87×10^{-2}). The performance of SetONet variants also degrades, with mean aggregation models showing particular sensitivity (relative L_2 errors of 2.00×10^{-1} and 2.21×10^{-1}). However, SetONet, processing the available sensors directly by design without requiring interpolation, again demonstrates greater robustness overall compared to DeepONet with imputation on this non-uniform grid. The attention-based SetONet models perform better, with the variant using no positional encoding and attention aggregation (PE: None, Agg: Att) achieving a relative L_2 error of 3.57×10^{-2} , lower than DeepONet’s result. This further supports the conclusion that SetONet’s set-based architecture provides inherent robustness to missing data that can outperform standard architectures augmented with interpolation, especially when the non-uniform sensor placement makes simple interpolation less effective.

4.2. 1D Darcy Flow

In this example, we aim to learn the nonlinear operator for a 1D Darcy system. The problem of interest can be written as

$$\frac{du}{dx} \left(-\kappa(u(x)) \frac{du}{dx} \right) = s(x), \quad x \in [0, 1], \quad (7)$$

where the solution-dependent permeability is $\kappa(u(x)) = 0.2 + u^2(x)$ and the input term is a Gaussian random field $s(x) \sim \mathcal{GP}$ defined as $s(x) \sim \text{GP}(0, k(x, x'))$ such that $k(x, x') = \sigma^2 \exp(-\|x - x'\|^2 / (2\ell_x^2))$, where $\ell_x = 0.04$, $\sigma^2 = 1.0$. Homogeneous Dirichlet boundary conditions $u(0) = u(1) = 0$ are considered at boundary points. The problem is obtained from [12] and we use a finite difference solver to generate the necessary data for the problem. We generate a total of 1000 different examples with a training and test split of 4 to 1.

Table 3: Comparison of Relative L2 Error for DeepONet and SetONet variants on the 1D Darcy problem benchmark. Models were trained with either variable (randomly resampled per batch) or fixed sensor locations. The final column shows performance under test-time sensor drop-off (10%) for models originally trained with fixed sensors.

Model	Variable Sensors	Fixed Sensors	Fixed w/ 10% Drop-off
DeepONet	-	6.17×10^{-2}	1.25×10^{-1}
SetONet (PE: Sin, Agg: Att)	2.13×10^{-1}	1.68×10^{-2}	2.15×10^{-1}
SetONet (PE: Sin, Agg: Mean)	2.12×10^{-1}	1.58×10^{-2}	2.15×10^{-1}
SetONet (PE: None, Agg: Att)	2.25×10^{-1}	3.00×10^{-2}	2.32×10^{-1}
SetONet (PE: None, Agg: Mean)	2.61×10^{-1}	4.04×10^{-2}	2.49×10^{-1}

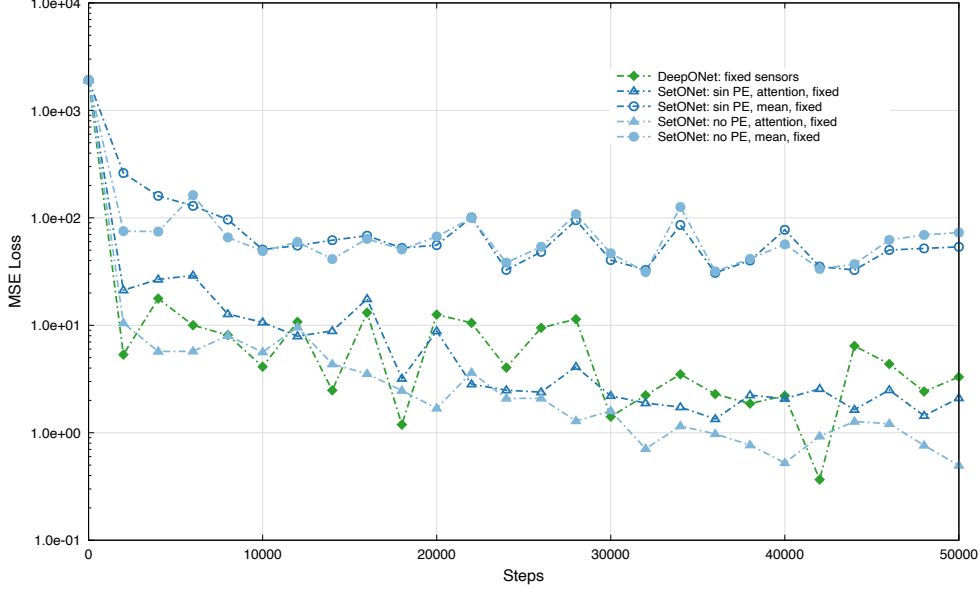


Figure 8: Test performance (Mean Squared Error Loss vs. Steps) for DeepONet and SetONet architectures on the Integral approximation benchmark, evaluated on a test set where 20% of sensors were randomly dropped out at test time only. All models were trained using fixed sensor locations per batch (dashed lines, "fixed"). The plot allows comparison of DeepONet against SetONet variants (incorporating different positional encoding (sinusoidal/none) and aggregation (attention/mean) methods) under this specific test condition with sensor dropout.

1D Darcy Flow Results

We now analyze the performance on the 1D Darcy flow problem, a nonlinear PDE where the operator maps the source term $s(x)$ to the solution $u(x)$. Variations in input were introduced through controlled sensor drop-off rather than resampling locations. Quantitative results are shown in Table 3, with loss curves in Figs. 10 and 11, and qualitative examples in Fig. 9.

Performance with Full Fixed Grid. First, we evaluate the baseline performance where models were trained and tested using the complete set of fixed sensor locations ("fixed" condition; Fig. 10 (a); Table 3, Col. 2). In this setting, which represents learning from complete information on the fixed grid, the SetONet architecture demonstrates a distinct advantage over standard DeepONet for this nonlinear problem. DeepONet achieves a relative L_2 error of 6.17×10^{-2} . In contrast, all SetONet variants yield lower relative L_2 errors, ranging from 1.58×10^{-2} to 4.04×10^{-2} . Optimal performance is achieved by SetONet configurations utilizing sinusoidal positional encoding (PE: Sin), with relative L_2 errors of 1.58×10^{-2} (Mean Aggregation) and 1.68×10^{-2} (Attention Aggregation). This result indicates that even when sensor locations are fixed, SetONet's architecture, particularly its capacity to leverage spatial information through PE, provides a benefit for approximating the solution operator of this nonlinear PDE compared to standard DeepONet. The qualitative predictions (Fig. 9) align with these findings, visually suggesting a closer match to the ground truth for SetONet.

Performance with Variable Sensors (Simulated via Drop-off). Next, we assess performance under variable sensor conditions, which for this fixed-grid Darcy problem were implemented by consistently applying a random 10% sensor drop-off during both training and testing for every sample. This experimental setup, designed to evaluate performance with varying input information derived from the fixed grid, corresponds to the "variable" condition in Fig. 10 (b) and the "Variable Sensors" column in Table 3 (Col. 1). Under this scenario, SetONet again significantly outperforms DeepONet. DeepONet fails to produce a converged relative L_2 error metric. All SetONet variants, however, achieve relative L_2 errors ranging from 2.12×10^{-1} to 2.61×10^{-1} . The configurations employing sinusoidal PE again demonstrate the best performance (relative L_2 errors of $\approx 2.1 \times 10^{-1}$), reinforcing the value of PE when dealing with

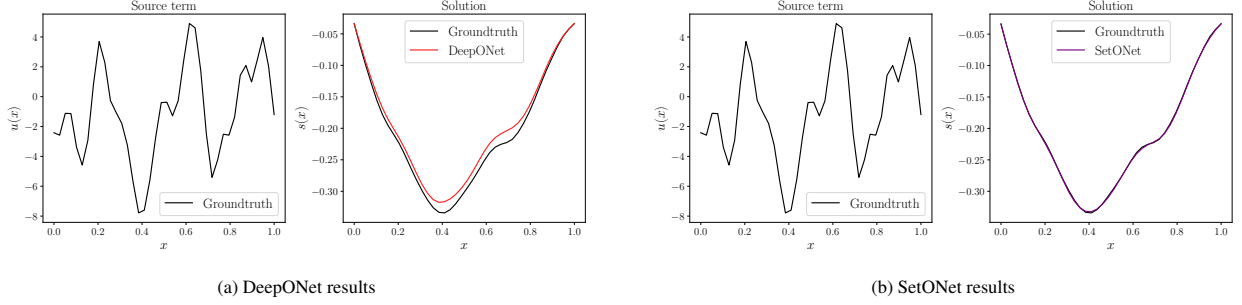


Figure 9: Comparison of example predictions for the 1D Darcy flow benchmark. Left (a): DeepONet prediction (red) vs. ground truth (black). Right (b): SetONet prediction (purple) vs. ground truth (black). The input source term $s(x)$ is shown in the left panel of each subfigure’s included graphic. When trained on the full fixed grid, SetONet shows slightly better qualitative agreement with the ground truth for this nonlinear problem.

incomplete input representations derived from the fixed grid. This experiment highlights SetONet’s enhanced robustness and learning capability compared to DeepONet when consistently trained and evaluated using reduced sensor sets from a fixed underlying grid.

Robustness to Sensor Drop-off at Test Time Only. The robustness to sensor drop-off occurring only at test time was assessed for the 1D Darcy flow problem. Models were trained on the complete fixed grid, but evaluated on test data where 10% of sensors were randomly removed (“Fixed w/ 10% Drop-off” condition; Fig. 11; Table 3, Col. 3). In this scenario, standard DeepONet, with missing sensor values estimated using linear interpolation enabled by the known fixed grid structure, achieves a relative L_2 error of 1.25×10^{-1} . This performance is notably better than all SetONet variants, whose relative L_2 errors range from 2.15×10^{-1} to 2.49×10^{-1} . SetONet processes the available data directly without interpolation, relying on its architecture. Similar to observations in other benchmarks, DeepONet’s stronger performance in this specific fixed-grid, test-time drop-off context appears linked to the effectiveness of linear interpolation when the underlying grid is fixed and known, allowing it to handle the variable missing data more successfully than the SetONet variants in this instance.

4.3. Elastic Plate

We test our approach on a commonly used benchmark problem that describes an elasticity model; variations of the same problem have been used in [12, 26].

In this example, we consider a rectangular plate with a center hole subjected to in-plane loading modeled as a two-dimensional problem of plane stress elasticity. The problem is governed by the equation

$$\nabla \cdot \boldsymbol{\sigma} + \mathbf{f}(\mathbf{x}) = 0, \quad \mathbf{x} = (x, y), \quad (8)$$

with boundary conditions

$$(u, v) = 0, \quad \forall \quad x = 0,$$

where $\boldsymbol{\sigma}$ is the Cauchy stress tensor, \mathbf{f} is the body force, $u(\mathbf{x})$ and $v(\mathbf{x})$ represent the x - and y -displacement, respectively. Additionally, we note that E , and ν represent the material’s Young modulus and Poisson ratio, respectively, and are fixed for the problem. The relation between stress and displacement in plane stress conditions is defined as:

$$\begin{bmatrix} \sigma_{xx} \\ \sigma_{yy} \\ \tau_{xy} \end{bmatrix} = \frac{E}{1 - \nu^2} \begin{bmatrix} 1 & \nu & 0 \\ \nu & 1 & 0 \\ 0 & 0 & \frac{1 - \nu}{2} \end{bmatrix} \times \begin{bmatrix} \frac{\partial u}{\partial x} \\ \frac{\partial v}{\partial y} \\ \frac{\partial u}{\partial y} + \frac{\partial v}{\partial x} \end{bmatrix}. \quad (9)$$

In this example, we model the loading conditions $\mathbf{f}(\mathbf{x})$ applied to the right edge of the plate as a Gaussian random field. Our goal for the task is to learn the mapping $\mathcal{T} : \mathbf{f}(\mathbf{x}) \rightarrow [u(\mathbf{x}), v(\mathbf{x})]$ from the random boundary load to the displacement field (u : x -displacement and v : y -displacement). We use the dataset for this problem made available in [12]. For our testing, we use $E = 300 \times 10^5$ and $\nu = 0.3$.

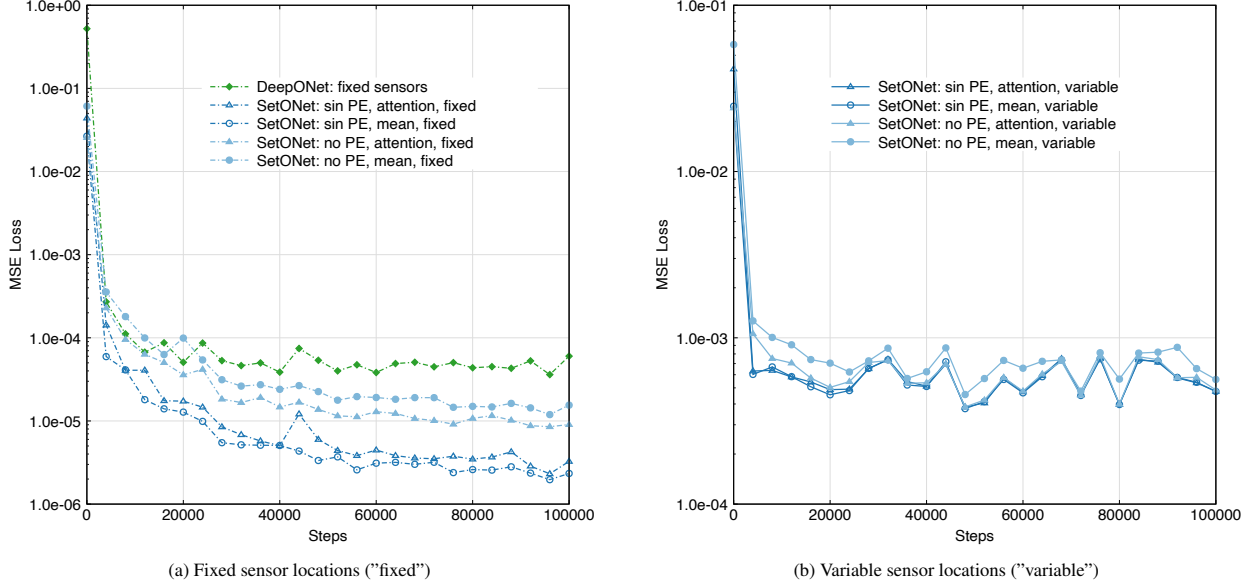


Figure 10: Test performance (Mean Squared Error Loss vs. Steps) for DeepONet and SetONet architectures on the 1D Darcy problem benchmark. (a) Results for models trained and evaluated using fixed sensor locations (dashed lines, "fixed") and a fixed evaluation grid size. (b) Results for models trained and evaluated using variable sensor locations (solid lines, "variable"), where sensor locations were randomly resampled for each batch. In both scenarios, the performance of DeepONet can be compared to SetONet variants incorporating different positional encoding (sinusoidal/none) and aggregation (attention/mean) methods.

Elastic Plate Results

We evaluate the models on the 2D Elastic Plate benchmark, where the operator maps a random boundary load $f(x)$ to the resulting displacement field $[u(x), v(x)]$. Input data for the forcing function is provided on a fixed grid. Quantitative results are presented in Table 4, with loss curves in Figs. 14 and 15, and qualitative examples in Figs. 12 and 13.

Performance with Full Fixed Grid. In the "fixed" condition using the complete set of fixed sensor locations (dashed lines, Fig. 14 (a); Table 4, Col. 2), both standard DeepONet and the SetONet variants achieve high accuracy. DeepONet obtains a relative L_2 error of 4.84×10^{-3} . The best-performing SetONet configurations utilize sinusoidal positional encoding (PE: Sin), achieving relative L_2 errors of 4.91×10^{-3} (Mean Aggregation) and 5.44×10^{-3} (Attention Aggregation). These results are very close to the DeepONet baseline, indicating that for this problem on a fixed grid, both DeepONet and optimally configured SetONet perform comparably well ("on par"). The variants without PE show notably higher relative L_2 errors (9.84×10^{-3} and 2.16×10^{-2}), suggesting PE is beneficial here even with fixed sensors. Qualitative results (Figs. 12, 13) show good agreement with the ground truth for both architectures, although error maps might reveal subtle differences.

Performance with Variable Sensors (Simulated via Drop-off). Similar to the Darcy flow setup, the "variable" sensor condition for this benchmark was implemented by applying a random 20% sensor drop-off during both training and testing for every sample ("variable" condition; Fig. 14 (b); Table 4, Col. 1). Under this persistent data reduction, SetONet demonstrates a significant advantage over DeepONet. DeepONet fails to produce a converged relative L_2 error metric. In contrast, all SetONet configurations maintain much lower relative L_2 errors, ranging from 8.77×10^{-2} to 2.00×10^{-1} . The best performance is achieved by the attention-based aggregation model without positional encoding (PE: None, Agg: Att variant yielding the lowest relative L_2 error of 8.77×10^{-2}), followed by models using sinusoidal PE (e.g., PE: Sin, Agg: Mean at 8.99×10^{-2} and PE: Sin, Agg: Att at 9.25×10^{-2}). This again underscores SetONet's superior ability to learn effectively from consistently incomplete data derived from a fixed grid compared to standard DeepONet.

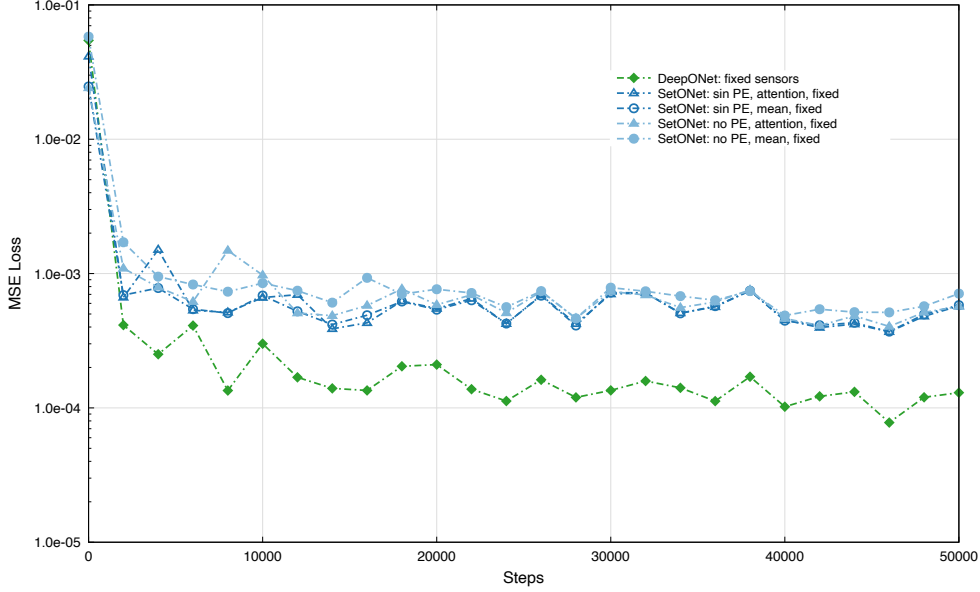


Figure 11: Test performance (Mean Squared Error Loss vs. Steps) for DeepONet and SetONet architectures on the 1D Darcy problem benchmark, evaluated on a test set where 10% of sensors were randomly dropped out at test time only. All models were trained using fixed sensor locations (dashed lines, “fixed”) and a fixed grid size. The plot allows comparison of DeepONet against SetONet variants (incorporating different positional encoding (sinusoidal/none) and aggregation (attention/mean) methods) under this specific test condition with sensor dropout.

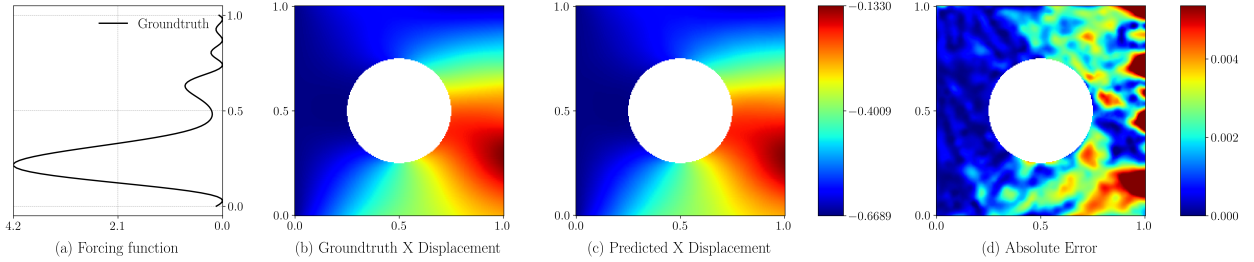


Figure 12: Example DeepONet results on the Elastic Plate problem benchmark with a circular inclusion. (a) Input forcing function. (b) Groundtruth horizontal displacement field. (c) Predicted displacement field by DeepONet. (d) Absolute error between prediction and ground truth.

Robustness to Sensor Drop-off at Test Time Only. We also assess robustness to data loss occurring only during inference. Models were trained on the complete fixed grid, but evaluated on test data where 20% of sensors were randomly removed (“Fixed w/ 20% Drop-off” condition; Fig. 15; Table 4, Col. 3). In this scenario, standard DeepONet, with missing sensor values estimated using linear interpolation enabled by the known fixed grid structure, achieves a relative L_2 error of 1.71×10^{-2} . This performance is markedly better (by roughly a factor of 5) than all SetONet variants, whose relative L_2 errors range from 8.68×10^{-2} to 1.94×10^{-1} . SetONet processes the available data directly without interpolation, relying on its architecture. As hypothesized for the Darcy problem, DeepONet’s strong performance here appears linked to the effectiveness of linear interpolation when the underlying grid is fixed and known, allowing it to successfully handle variable missing data at test time better than the SetONet variants in this specific fixed-grid context.

4.4. Summary of Experimental Results

Our experimental evaluations across several benchmarks highlight the capabilities and advantages of the SetONet architecture compared to standard DeepONet.

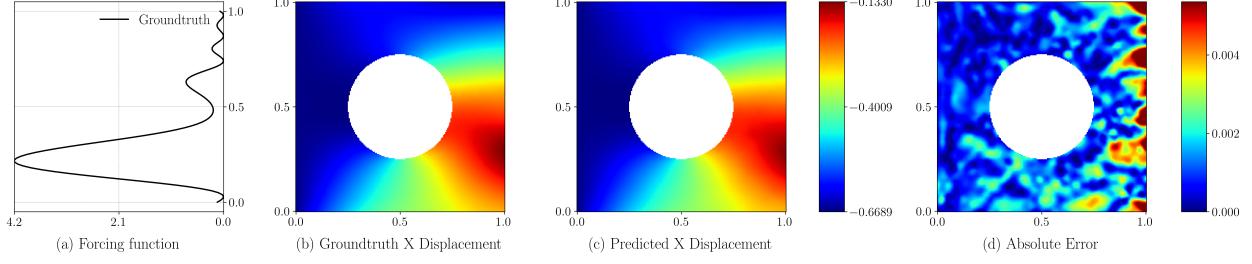


Figure 13: Example SetONet results on the Elastic Plate problem benchmark with a circular inclusion. (a) Input forcing function. (b) Ground-truth horizontal displacement field. (c) Predicted displacement field by SetONet. (d) Absolute error between prediction and ground truth.

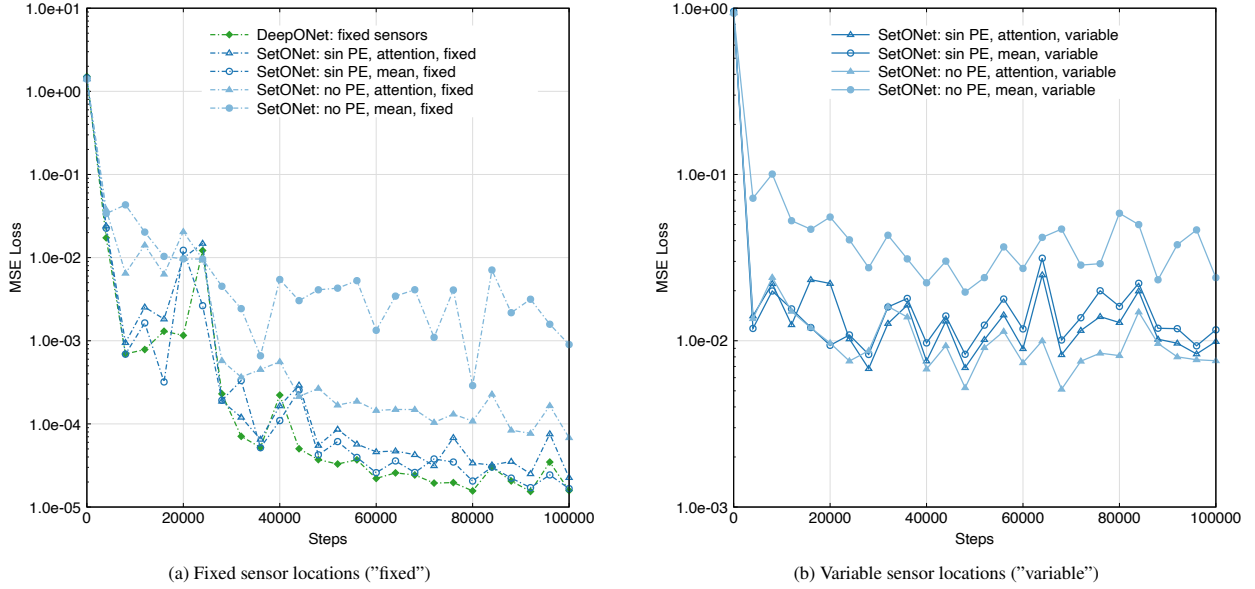


Figure 14: Test performance (Mean Squared Error Loss vs. Steps) for DeepONet and SetONet architectures on the Elastic Plate problem benchmark. (a) Results for models trained and evaluated using fixed sensor locations (dashed lines, "fixed") and a fixed evaluation grid size. (b) Results for models trained and evaluated using variable sensor locations (solid lines, "variable"), where sensor locations were randomly resampled for each batch. In both scenarios, the performance of DeepONet can be compared to SetONet variants incorporating different positional encoding (sinusoidal/none) and aggregation (attention/mean) methods.

On fundamental operator learning tasks (derivative/anti-derivative), SetONet demonstrated high accuracy under ideal conditions with fixed, consistent sensor locations, performing essentially on par with the strong DeepONet baseline. However, the primary strength of SetONet became evident in more challenging scenarios. When sensor locations were varied per training batch, or when sensors were missing during inference (drop-off), SetONet significantly outperformed standard DeepONet. In these variable or incomplete data regimes, DeepONet's performance collapsed due to its reliance on a fixed input structure. In contrast, SetONet's permutation-invariant design and explicit handling of location-value pairs enabled it to maintain high accuracy and robustness. These initial tests also indicated that sinusoidal positional encoding could be beneficial when sensor locations varied dynamically, and attention-based aggregation often provided enhanced robustness compared to mean pooling, especially under sensor drop-off conditions.

The 1D Darcy flow benchmark provided further insights for a nonlinear PDE operator. Notably, SetONet, particularly when utilizing sinusoidal positional encoding, demonstrated superior accuracy to standard DeepONet, even when both models were trained and tested on the complete, fixed sensor grid. This advantage is likely attributable to SetONet's branch network design, which explicitly processes both location (x_i) and value (u_i) information jointly, potentially allowing it to capture complex nonlinear dependencies more effectively. Furthermore, SetONet exhibited significantly enhanced robustness when faced with persistent data scarcity (simulated via 10% drop-off during train-

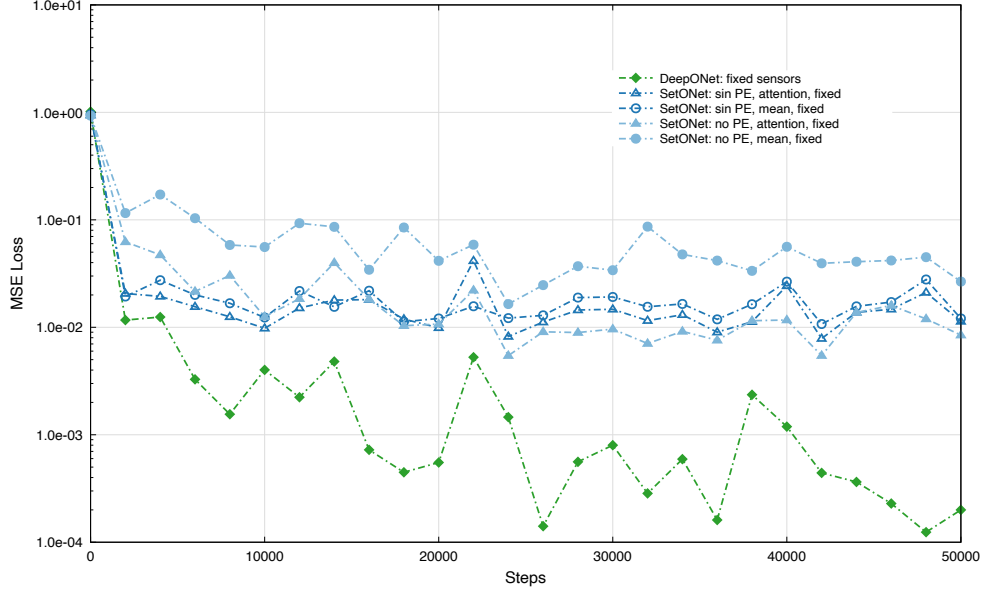


Figure 15: Test performance (Mean Squared Error Loss vs. Steps) for DeepONet and SetONet architectures on the Elastic Plate problem benchmark, evaluated on a test set where 20% of sensors were randomly dropped out at test time only. All models were trained using fixed sensor locations (“fixed”). The plot allows comparison of DeepONet against SetONet variants (incorporating different positional encoding (sinusoidal/none) and aggregation (attention/mean) methods) under this specific test condition with sensor dropout.

Table 4: Comparison of Relative L2 Error for DeepONet and SetONet variants on the Elastic Plate problem benchmark. Models were trained with either variable (randomly resampled per batch) or fixed sensor locations. The final column shows performance under test-time sensor drop-off (20%) for models originally trained with fixed sensors.

Model	Variable Sensors	Fixed Sensors	Fixed w/ 20% Drop-off
DeepONet	-	4.84×10^{-3}	1.71×10^{-2}
SetONet (PE: Sin, Agg: Att)	9.25×10^{-2}	5.44×10^{-3}	9.17×10^{-2}
SetONet (PE: Sin, Agg: Mean)	8.99×10^{-2}	4.91×10^{-3}	9.04×10^{-2}
SetONet (PE: None, Agg: Att)	8.77×10^{-2}	9.84×10^{-3}	8.68×10^{-2}
SetONet (PE: None, Agg: Mean)	2.00×10^{-1}	2.16×10^{-2}	1.94×10^{-1}

ing and testing). However, when sensor drop-off occurred only at test time, standard DeepONet, augmented with linear interpolation enabled by the known fixed grid, achieved slightly better accuracy than SetONet. This highlights SetONet’s advantages for capturing nonlinear operators and handling consistent data sparsity, while underscoring that DeepONet’s robustness to variable test-time drop-off in this fixed-grid context can be effectively aided by imputation.

The 2D Elastic Plate benchmark further clarified these comparative strengths. On the complete fixed grid, DeepONet and the best SetONet configurations (utilizing sinusoidal PE) performed comparably. Again, SetONet demonstrated significantly better robustness and accuracy when trained and tested under persistent data sparsity conditions (simulated via 20% drop-off). However, consistent with the Darcy flow results, when data loss occurred only at test time, DeepONet, aided by linear interpolation on the known fixed grid, substantially outperformed SetONet.

In summary, SetONet offers comparable performance to DeepONet in fixed input settings but provides crucial robustness and flexibility required for scenarios involving variable input sampling or consistent data sparsity, where it substantially surpasses the standard architecture. Its ability to explicitly process location-value pairs also appears beneficial for certain nonlinear problems, even on fixed grids. While standard DeepONet, coupled with imputation, can be effective for variable data loss on known fixed grids, SetONet’s architectural design makes it inherently suited for applications where input variability or incompleteness is expected.

5. Conclusion

In this work, we introduced the Set Operator Network (SetONet), a novel neural operator architecture designed to address a key limitation of the standard Deep Operator Network (DeepONet): its reliance on input functions sampled at fixed locations. The core innovation of SetONet lies in its branch network design, which leverages principles from Deep Sets to process input data as an unordered *set* of location-value pairs $\{(\mathbf{x}_i, g(\mathbf{x}_i))\}_{i=1}^M$. By explicitly incorporating both sensor locations \mathbf{x}_i and sensor values $g(\mathbf{x}_i)$ and ensuring permutation invariance through the Deep Sets methodology, SetONet can naturally handle variations in the number (M) and locations (\mathbf{x}_i) of input sensors. This capability is crucial for practical applications involving experimental data, irregular discretizations, or scenarios where sensor configurations change.

Our experimental results across several benchmark problems, including derivative/anti-derivative operators, 1D Darcy flow, and 2D elasticity, demonstrate the effectiveness and robustness of SetONet. We showed that SetONet successfully learns operator mappings in scenarios with variable sensor locations sampled per batch, conditions under which standard DeepONet fails due to its architectural constraints. Furthermore, SetONet exhibited significant robustness to sensor drop-off. When sensor data was missing (simulated via drop-off), SetONet, processing the available incomplete set directly, often outperformed standard DeepONet, even when the latter was augmented with interpolation techniques, particularly when interpolation was challenged by non-uniform sensor distributions or when sparsity was present during training.

Interestingly, our findings also revealed that SetONet can achieve performance comparable to, or even exceeding, standard DeepONet on tasks with fixed input grids. For the nonlinear 1D Darcy flow problem, SetONet variants consistently achieved lower errors than DeepONet, potentially due to the SetONet branch’s explicit processing of both spatial coordinates and function values, allowing it to capture complex spatial dependencies more effectively. We investigated different architectural choices within SetONet, finding that sinusoidal positional encoding often proved beneficial, especially when sensor locations varied dynamically or for problems with significant spatial structure (like Darcy flow), while attention-based aggregation generally offered improved robustness over simple mean aggregation, particularly under sensor drop-off conditions. However, we also noted specific scenarios, such as variable sensor drop-off at test time on a known fixed grid, where DeepONet combined with linear interpolation could outperform SetONet, highlighting the effectiveness of imputation when grid structure can be leveraged.

The SetONet framework offers a flexible and robust approach for operator learning in settings characterized by variable or incomplete input data, enabled by its unique branch network design that processes location-value pairs invariantly. Future research could explore the application of SetONet to a wider range of complex, high-dimensional PDE systems and real-world datasets with inherent input variability. Further investigations could focus on optimizing architectural components, such as exploring alternative positional encoding schemes or more sophisticated attention mechanisms within the aggregation layer. Crucially, the ability of the SetONet branch to process richer inputs beyond just values presents exciting avenues. Future work should explore leveraging this capability by feeding triplets like $(\mathbf{x}_i, g(\mathbf{x}_i), \text{property}(\mathbf{x}_i))$, allowing the model to handle spatially varying properties within the input domain directly. Additionally, exploring other potential advantages inherent in processing location-value pairs, such as improved capabilities for interpolation, extrapolation, or directly learning from boundary condition data, represents a promising direction. Comparing SetONet theoretically and empirically against other emerging variable-input neural operators is also essential. Overall, SetONet provides a valuable extension to the neural operator toolkit, enhancing applicability to problems where input data structure is not fixed a priori.

Acknowledgments

This work was funded in part by NSF 2339678 and 2438193. Any opinions, findings, conclusions, or recommendations expressed in this material are those of the author(s) and do not necessarily reflect the views of the funding organizations. We would like to express my heartfelt gratitude to Dr. Somdatta Goswami at Johns Hopkins University for her insightful discussions that greatly enriched this work.

References

- [1] N. Kovachki, Z. Li, B. Liu, K. Azizzadenesheli, K. Bhattacharya, A. Stuart, A. Anandkumar, Neural operator: Learning maps between function spaces with applications to pdes, *Journal of Machine Learning Research* 24 (89) (2023) 1–97.

- [2] L. Lu, P. Jin, G. Pang, Z. Zhang, G. E. Karniadakis, Learning nonlinear operators via deepnet based on the universal approximation theorem of operators, *Nature machine intelligence* 3 (3) (2021) 218–229.
- [3] T. Chen, H. Chen, Universal approximation to nonlinear operators by neural networks with arbitrary activation functions and its application to dynamical systems, *IEEE transactions on neural networks* 6 (4) (1995) 911–917.
- [4] Z. Li, N. Kovachki, K. Azizzadenesheli, B. Liu, K. Bhattacharya, A. Stuart, A. Anandkumar, Fourier neural operator for parametric partial differential equations (2021). *arXiv*:2010.08895.
URL <https://arxiv.org/abs/2010.08895>
- [5] T. Tripura, S. Chakraborty, Wavelet neural operator: a neural operator for parametric partial differential equations (2022). *arXiv*:2205.02191.
URL <https://arxiv.org/abs/2205.02191>
- [6] A. Anandkumar, K. Azizzadenesheli, K. Bhattacharya, N. Kovachki, Z. Li, B. Liu, A. Stuart, Neural operator: Graph kernel network for partial differential equations, in: *ICLR 2020 workshop on integration of deep neural models and differential equations*, 2020.
- [7] Q. Cao, S. Goswami, G. E. Karniadakis, Laplace neural operator for solving differential equations, *Nature Machine Intelligence* 6 (6) (2024) 631–640.
- [8] Z. Li, K. Meidani, A. B. Farimani, Transformer for partial differential equations’ operator learning, *arXiv preprint arXiv:2205.13671* (2022).
- [9] Z. Hao, Z. Wang, H. Su, C. Ying, Y. Dong, S. Liu, Z. Cheng, J. Song, J. Zhu, Gnot: A general neural operator transformer for operator learning, in: *International Conference on Machine Learning*, PMLR, 2023, pp. 12556–12569.
- [10] L. Lu, P. Jin, G. E. Karniadakis, Deepnet: Learning nonlinear operators for identifying differential equations based on the universal approximation theorem of operators, *arXiv preprint arXiv:1910.03193* (2019).
- [11] M. Prasthofer, T. De Ryck, S. Mishra, Variable-input deep operator networks, *arXiv preprint arXiv:2205.11404* (2022).
- [12] T. Ingebrand, A. J. Thorpe, S. Goswami, K. Kumar, U. Topcu, Basis-to-basis operator learning using function encoders, *Computer Methods in Applied Mechanics and Engineering* 435 (2025) 117646.
- [13] M. Zaheer, S. Kottur, S. Ravanbakhsh, B. Poczos, R. Salakhutdinov, A. Smola, Deep sets (2018). *arXiv*:1703.06114.
URL <https://arxiv.org/abs/1703.06114>
- [14] Y. Zhu, S. Kitajima, N. Nishizawa, A fast prediction framework for multi-variable nonlinear dynamic modeling of fiber pulse propagation using deepnet, *Applied Sciences* 14 (18) (2024) 8154.
- [15] Z. Xiao, Z. Hao, B. Lin, Z. Deng, H. Su, Improved operator learning by orthogonal attention, *arXiv preprint arXiv:2310.12487* (2023).
- [16] T. Wang, C. Wang, Latent neural operator for solving forward and inverse pde problems, *arXiv preprint arXiv:2406.03923* (2024).
- [17] S. Li, C. Liu, H. Ni, Enhancing neural operator learning with invariants to simultaneously learn various physical mechanisms, *National Science Review* 11 (8) (2024) nwae198.
- [18] M. A. Rahman, R. J. George, M. Elleithy, D. Leibovici, Z. Li, B. Bonev, C. White, J. Berner, R. A. Yeh, J. Kossaifi, et al., Pretraining codomain attention neural operators for solving multiphysics pdes, *Advances in Neural Information Processing Systems* 37 (2024) 104035–104064.
- [19] G. Kissas, J. H. Seidman, L. F. Guilhoto, V. M. Preciado, G. J. Pappas, P. Perdikaris, Learning operators with coupled attention, *Journal of Machine Learning Research* 23 (215) (2022) 1–63.
- [20] B. Bahmani, S. Goswami, I. G. Kevrekidis, M. D. Shields, A resolution independent neural operator (2024). *arXiv*:2407.13010.
URL <https://arxiv.org/abs/2407.13010>
- [21] Z. Li, N. Kovachki, K. Azizzadenesheli, B. Liu, K. Bhattacharya, A. Stuart, A. Anandkumar, Neural operator: Graph kernel network for partial differential equations, *arXiv preprint arXiv:2003.03485* (2020).
- [22] S. W. Cho, J. Y. Lee, H. J. Hwang, Learning time-dependent pde via graph neural networks and deep operator network for robust accuracy on irregular grids, *arXiv preprint arXiv:2402.08187* (2024).
- [23] A. Peyvan, V. Kumar, Fusion deepnet: A data-efficient neural operator for geometry-dependent hypersonic flows on arbitrary grids, *arXiv preprint arXiv:2501.01934* (2025).
- [24] A. Vaswani, N. Shazeer, N. Parmar, J. Uszkoreit, L. Jones, A. N. Gomez, L. Kaiser, I. Polosukhin, Attention is all you need (2017). *arXiv*:1706.03762.
URL <https://arxiv.org/abs/1706.03762>
- [25] J. Lee, Y. Lee, J. Kim, A. Kosiorek, S. Choi, Y. W. Teh, Set transformer: A framework for attention-based permutation-invariant neural networks, in: K. Chaudhuri, R. Salakhutdinov (Eds.), *Proceedings of the 36th International Conference on Machine Learning*, Vol. 97 of *Proceedings of Machine Learning Research*, PMLR, 2019, pp. 3744–3753.
URL <https://proceedings.mlr.press/v97/lee19d.html>
- [26] S. Goswami, K. Kontolati, M. D. Shields, G. E. Karniadakis, Deep transfer operator learning for partial differential equations under conditional shift, *Nature Machine Intelligence* 4 (12) (2022) 1155–1164.